

Dimer Models and Integrable Systems

Richard Eager^{1,2}, Sebastián Franco³ and Kevin Schaeffer⁴

¹*Department of Physics, University of California, Santa Barbara, CA 93106, USA*

²*Institute for the Physics and Mathematics of the Universe, University of Tokyo
Kashiwa, Chiba 277-8582, Japan*

³*Kavli Institute for Theoretical Physics, University of California
Santa Barbara, CA 93106, USA*

⁴*Center for Theoretical Physics, Department of Physics, University of California
Berkeley, CA 94720, USA*

`richard.eager@ipmu.jp`, `sebastian.franco@durham.ac.uk`

ABSTRACT: We explore various aspects of the correspondence between dimer models and integrable systems recently introduced by Goncharov and Kenyon. Dimer models give rise to relativistic integrable systems that match those arising from 5d $\mathcal{N} = 1$ gauge theories studied by Nekrasov. We apply the correspondence to dimer models associated to the $Y^{p,0}$ geometries, showing that they give rise to the relativistic generalization of the periodic Toda chain originally studied by Ruijsenaars. The correspondence reduces the calculation of all conserved charges to a straightforward combinatorial problem of enumerating non-intersecting paths in the dimer model. We show how the usual periodic Toda chain emerges in the non-relativistic limit and how the Lax operator corresponds to the Kasteleyn matrix of the dimer model. We discuss how the dimer models for general $Y^{p,q}$ manifolds give rise to other relativistic integrable systems, generalizing the periodic Toda chain and construct the integrable systems for general $Y^{p,p}$ explicitly. The impurities introduced in the construction of $Y^{p,q}$ quivers are identified with impurities in twisted $\mathfrak{sl}(2)$ XXZ spin chains. Finally we discuss how the physical concept of higgsing a dimer model provides an efficient method for producing new integrable systems starting from known ones. We illustrate this idea by constructing the integrable systems for higgsings of $Y^{4,0}$.

Contents

1. Introduction	1
2. Some Background	2
3. Integrable Systems from Dimers, 5d and 4d	5
4. The Periodic Toda Chain	6
4.1 $Y^{p,0}$ Integrable Systems	7
4.2 Kasteleyn matrix	9
4.2.1 Non-Relativistic Limit	11
4.2.2 Loop Poisson Brackets from Edges	11
4.3 More Relativistic Generalizations of Toda from $Y^{p,q}$	12
4.4 $Y^{p,p}$ Integrable Systems	14
4.5 $Y^{p,q}$ Integrable Systems as Spin Chains	15
5. Generating New Integrable Systems via Partial Resolution	17
5.1 Examples: Partial Resolutions of $Y^{4,0}$	18
6. Conclusions and Outlook	23

1. Introduction

Integrable systems have a dense web of connections with gauge theories and string theory. Integrable systems appear in a variety of contexts including Seiberg-Witten theory [1], recent connections to the vacua of supersymmetric theories [2], and the calculation of the spectrum of anomalous dimensions [3] and scattering amplitudes [4] in super-Yang-Mills, to name a few.

Recently, Goncharov and Kenyon discovered an exciting correspondence between integrable systems and dimer models [5]. According to their correspondence, every dimer model defines an integrable system, whose conserved charges can be systematically calculated from perfect matchings.

The correspondence sheds new light on integrable systems, with applications and implications yet to be investigated. It provides new perspectives on integrable systems that are naturally related to dimer models, such as 4d quiver gauge theories, D3-branes probing toric Calabi-Yau 3-folds [6], mirror symmetry [7] and quantum Teichmüller space [5, 8].

In this paper, we investigate various aspects of the correspondence from a physical perspective. This work is organized as follows. Section 2 briefly reviews the relation between dimer models and quiver theories, toric Calabi-Yaus and integrable systems. Section 3 discusses the connection between integrable systems and 5d $\mathcal{N} = 1$ and 4d $\mathcal{N} = 2$ gauge theories. In Section 4, we apply the correspondence, constructing a relativistic generalization of the periodic Toda chain from the dimer models associated to $Y^{p,0}$ manifolds. We study the relation between the Kasteleyn and Lax operators, the non-relativistic limit of the integrable system and how dimer models for general $Y^{p,q}$ geometries produce alternative relativistic generalizations of the periodic Toda chain. We also discuss the connection to twisted $\mathfrak{sl}(2)$ XXZ spin chains with impurities. In Section 5, we introduce a practical method for generating new integrable systems based in higgsing and illustrate the method with explicit examples. We conclude and mention future directions in Section 6.

2. Some Background

In this section we provide a lightning review of various concepts used throughout this paper. When necessary, we indicate references for more thorough explanations.

Dimers and Quivers

Brane tilings, to which we will also refer to as dimer models, are bipartite graphs embedded in a two-torus. The dual of a brane tiling is a planar, periodic quiver. There is a one-to-one correspondence between brane tilings and periodic quivers [6] that is summarized in the following dictionary:

Gauge Theory		Brane Tiling
gauge group	\leftrightarrow	face
chiral superfield	\leftrightarrow	edge
superpotential term	\leftrightarrow	node

Every term in the superpotential of the gauge theory is encoded in an oriented plaquette of the periodic quiver. Figure 1 exemplifies the correspondence for phase I of F_0 [9].

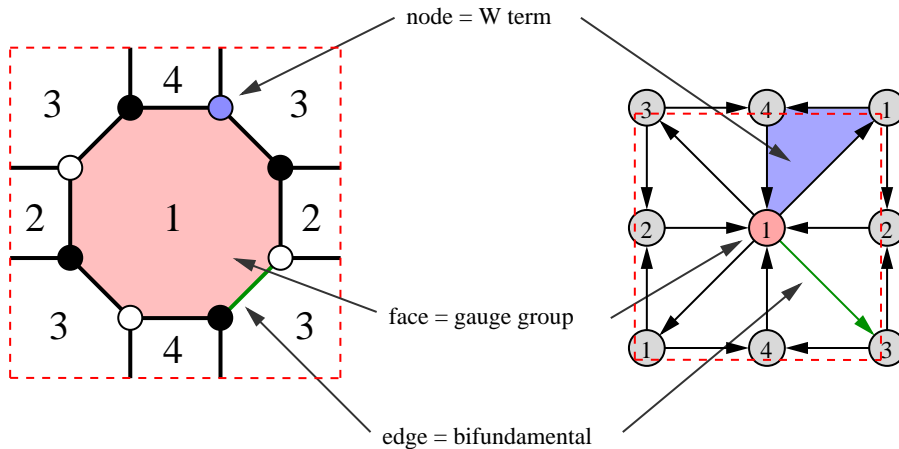


Figure 1: Correspondence between the brane tiling and the periodic quiver for phase I of F_0 .

Dimers and Calabi-Yau 3-folds

Quiver gauge theories that are described by brane tilings arise on the worldvolume of stacks of D3-branes probing singular, toric Calabi-Yau (CY) 3-folds. The CY geometry emerges as the moduli space of vacua of the quiver gauge theory. The connection between dimer models and quivers has trivialized the determination of the corresponding CY geometry. GLSM fields in the toric description of the CY are in one-to-one correspondence with perfect matchings of the dimer model. As a result, points in the toric diagram correspond to (sets of) perfect matchings. This correspondence reduces the task of finding the CY geometry to computing the determinant of the Kasteleyn matrix [6].

Dimers and Integrable Systems

The dynamical variables of the integrable system correspond to oriented loops in the brane tiling. One basis for such loops is given by the cycles going clockwise around each face w_i ($i = 1, \dots, N_g$, with N_g the number of gauge groups in the quiver) and the cycles z_1 and z_2 wrapping the two directions of the 2-torus.^{1,2}

¹Since $\prod_{i=1}^{N_g} w_i = 1$, one of the w_i 's is redundant. This identity can also be exploited for simplifying expressions.

²The analysis of some models, such as the ones in Section 4, can be considerably simplified by choosing a different basis.

The Poisson brackets between basis cycles are

$$\begin{aligned}\{w_i, w_j\} &= \epsilon_{w_i, w_j} w_i w_j \\ \{z_1, z_2\} &= (\langle z_1, z_2 \rangle + \epsilon_{z_1, z_2}) z_1 z_2 \\ \{z_a, w_i\} &= \epsilon_{z_a, w_i} z_a w_i\end{aligned}\tag{2.1}$$

where $\epsilon_{x,y}$ is the number of edges on which the loops x and y overlap, counted with orientation. Then, ϵ_{w_i, w_j} is simply the antisymmetric oriented incidence matrix of the quiver. In addition, $\langle z_1, z_2 \rangle$ is the intersection number in homology of the cycles z_1 and z_2 .

The classical integrable system can be quantized replacing the Poisson brackets by a q -deformed algebra of the form

$$X_i X_j = q^{\{x_i, x_j\}} X_j X_i,\tag{2.2}$$

where $X_i = e^{x_i}$ and $q = e^{-i2\pi\hbar}$.

Every perfect matching corresponds to a point in the toric diagram and defines a closed loop by subtraction of a reference perfect matching. This loop can then be expressed in terms of the basic cycles. When multiple perfect matchings correspond to a given toric diagram point, their contributions must be added. Goncharov and Kenyon showed that the commutators defined by (2.2) and (2.1) result in a $(0+1)$ -dimensional quantum integrable system in which the conserved charges are given by:

- **Casimirs:** they commute with everything. They are defined as the ratio between contributions of consecutive points on the boundary of the toric diagram.
- **Hamiltonians:** they commute with each other and correspond to internal points in the toric diagram.

In this paper we will not discuss the choice of reference perfect matching in detail, we instead refer the interested reader to [5]. Different choices of the reference perfect matching correspond to shifts in the toric diagram. These overall shifts do not affect Casimirs (since they are defined as ratios of points in the toric diagram) but they modify the Hamiltonian(s). Models with zero or one internal point are insensitive to this choice, since they have zero or one Hamiltonians. The choice of reference perfect matching becomes important for models with more than one internal point and can be straightforwardly determined by demanding the Hamiltonians to commute.

Following [10] (see also [11] for applications), we define the magnetic flux through a loop, γ , in terms of edges in the tiling as

$$v(\gamma) = \prod_{i=1}^{k-1} \frac{X(\mathbf{w}_i, \mathbf{b}_i)}{X(\mathbf{w}_{i+1}, \mathbf{b}_i)}, \quad (2.3)$$

where the product runs over the contour γ and \mathbf{b}_i and \mathbf{w}_j denote black and white nodes. With this definition, the elements in our basis are $w_j \equiv v(\gamma_{w_j})$, $z_1 \equiv v(\gamma_{z_1})$, and $z_2 \equiv v(\gamma_{z_2})$. Another brief but more complete summary of the work in [5] can be found in [8].

3. Integrable Systems from Dimers, 5d and 4d

5d Gauge Theories and Dimers

The integrable systems we are discussing can be derived from either dimer models or 5d gauge theories. The main object underlying all constructions is the spectral curve Σ .

Dimer models encode the quiver gauge theory (and also the geometry) on D3-branes probing a singular, toric Calabi-Yau 3-fold X . The toric singularity has a characteristic polynomial $P(z_1, z_2) = \sum a_{n_1, n_2} z_1^{n_1} z_2^{n_2}$, where (n_1, n_2) runs over points in the toric diagram. The mirror Calabi-Yau is given by $P(z_1, z_2) = W$, $W = uv$. In this case, Σ corresponds to the Riemann surface sitting at $W = 0$ in the mirror.

Nekrasov [12] proposed a non-perturbative solution for 5d gauge theories compactified on a circle using relativistic integrable systems. From the Seiberg-Witten solution [13, 14] a connection to integrable systems was proposed in [1]. In particular, the spectral curve of the integrable system matches the Seiberg-Witten curve. Nekrasov's insight was to generalize the integrable system to a relativistic integrable system in order to determine the corresponding Seiberg-Witten curve for the 5d gauge theory. There are two possible ways to engineer such compactified 5d theories and Σ plays a prominent role in both of them. First, we can construct them by wrapping an M5-brane on Σ . This M5-brane is a de-singularization of a web of (p, q) 5-branes in Type IIB, obtained after compactifying in a circle of radius β to pass to Type IIA and then lifting to M-theory [15]. Alternatively, these theories can be obtained in the low energy limit of M-theory on a Calabi-Yau 3-fold with vanishing cycles to decouple gravity [16, 17, 18, 19]. The Calabi-Yau is the same X of the dimer construction, so we see that Σ is also relevant from this perspective. Particle-like states arise from M2-branes wrapped around SUSY 2-cycles.

4d Gauge Theories and the Non-Relativistic Limit

The integrable systems constructed using dimer models (equivalently 5d gauge theories compactified on a circle) are naturally *relativistic*. This is reflected, for example, in the exponential dependence on momenta of the conserved charges. This fact is manifest in the form of Poisson brackets (2.1).

The radius, β , of the circle on which the 5d gauge theory is compactified plays the role of the inverse speed of light. The non-relativistic limit corresponds to taking $\beta \rightarrow 0$.³ In this limit, we obtain a 4d, $\mathcal{N} = 2$ gauge theory whose Seiberg-Witten curve is the spectral curve of the non-relativistic integrable system, which we denote σ .⁴ Figure 2 summarizes the connection between 5d gauge theories, dimer models, integrable systems and their non-relativistic (4d) limits.

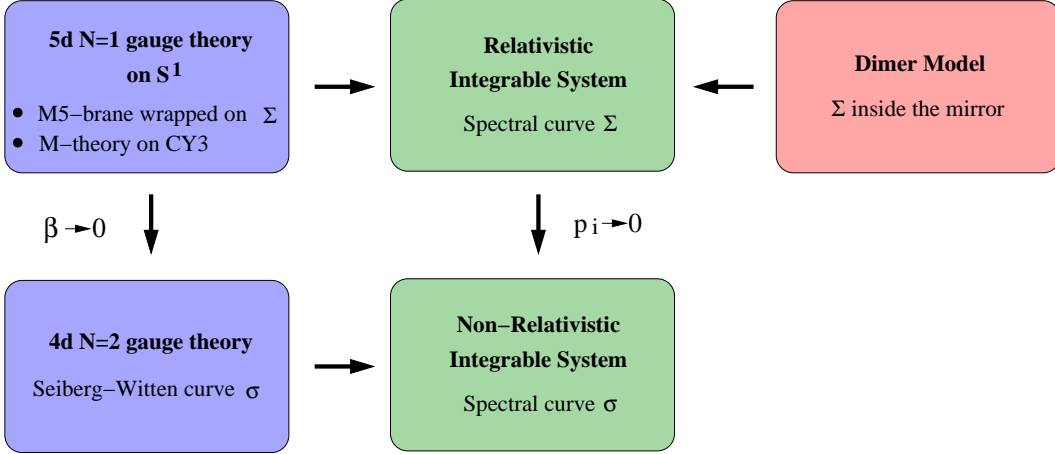


Figure 2: Dimer models and 5d, $\mathcal{N} = 1$ gauge theories compactified on an S^1 correspond to different perspectives on the spectral curve Σ . The 4d, $\mathcal{N} = 2$ limit of the gauge theory corresponds to a non-relativistic limit of the integrable system.

4. The Periodic Toda Chain

In this section we show the correspondence from [5] at work in explicit examples, using

³Also interesting is the decompactification limit $\beta \rightarrow \infty$, in which the 5d perturbative solution [20] is recovered

⁴As explained in Section 2, dimer models are in one-to-one correspondence with 4d (generically $\mathcal{N} = 1$) quiver theories. These quivers thus provide other 4d gauge theories naturally associated to the integrable systems. In what follows, whether we refer to the 4d $\mathcal{N} = 2$ or quiver gauge theories should be clear from the context.

dimer models to construct (relativistic generalizations of) the periodic Toda chain. The relativistic, periodic Toda chain was first introduced in [21] and studied in connection with 5d gauge theories in [12]. These integrable systems arise from dimer models, equivalently quiver gauge theories, associated to $Y^{p,q}$ manifolds [22]. The associated spectral curves, Σ , correspond to 5d, $\mathcal{N} = 1$, $SU(p)$ gauge theory with no flavors and different values of a quantized parameter controlling the cubic couplings in the prepotential.

4.1 $Y^{p,0}$ Integrable Systems

Integrable system

Let us now consider general $Y^{p,0}$ geometries. Our goal is to make contact with the relativistic Toda chain for arbitrary p . For concreteness, let us focus on the case in which p is even. The shape of the unit cell depends on whether p is even (rectangle) or odd (rhombus). The dimer model for the conifold corresponds to a square lattice [23]. The cone over $Y^{p,0}$ is a \mathbb{Z}_p orbifold of the conifold. As a result, its dimer model is given by a square lattice with an enlarged unit cell, given by p copies of the one for the conifold, as shown in Figure 3.⁵

The reference perfect matching and z_1 and z_2 paths for $Y^{p,0}$ are shown in Figure 4. Figure 5 shows the toric diagram for $Y^{p,0}$, with even p . The system has a \mathbb{Z}_2 symmetry corresponding to choosing the opposite corner of the toric diagram as the reference perfect matching. The \mathbb{Z}_2 symmetry interchanges the Hamiltonian with its dual [27].

The construction of the associated integrable system is considerably simplified by an appropriate choice of basis of $2p + 2$ cycles, instead of w_i and z_j . Figure 6 shows $2p$ of the loops. There are two additional cycles, with winding numbers $(-p/2 - 1, 1)$ and $(-p/2 - 1, -1)$ around the z_1 and z_2 directions, which correspond to the green points in Figure 5. They are mapped to two Casimirs and are hence fixed.

The non-vanishing Poisson brackets are

$$\{c_k, d_k\} = c_k d_k \quad \{c_k, d_{k+1}\} = -c_k d_{k+1} \quad \{c_k, c_{k+1}\} = -c_k c_{k+1} \quad (4.1)$$

The Hamiltonian corresponds to the $(-1, 0)$ point in the toric diagram and is given by

$$H_1 = \sum_{i=1}^p (c_i + d_i). \quad (4.2)$$

⁵A similar configuration for a discrete time integrable system related to dimer models was considered in [25].

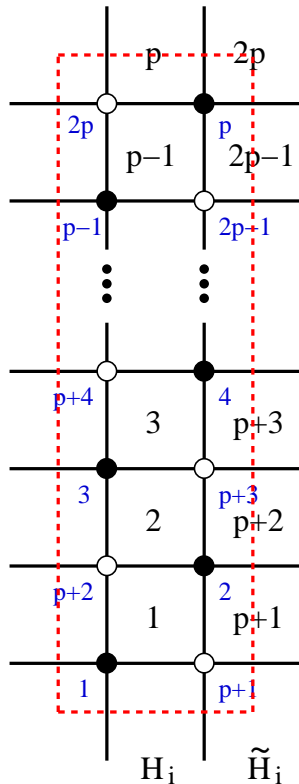


Figure 3: Brane tiling for $Y^{p,0}$ with even p . We indicate the numbering of nodes in blue.

Equations (4.1) and (4.2) precisely agree with the Poisson brackets and Hamiltonian for the general periodic relativistic Toda chain [26, 27]. The c_i and d_i variables can be expressed in terms of position and momentum variables with canonical commutation relations as follows

$$\begin{aligned}
 c_i &= \exp(p_i - q_i + q_{i+1}) \\
 d_i &= \exp p_i.
 \end{aligned}
 \tag{4.3}$$

Using the c_i and d_i cycles, determining the additional $(p - 2)$ higher Hamiltonians reduces to a straightforward combinatorial problem. The H_n Hamiltonian, associated with the $(-n, 0)$ point in the toric diagram, corresponds to the sum of all possible combinations of n of these cycles with the condition that they do not overlap or touch at any vertex of the tiling. For example, for $Y^{4,0}$ we have:

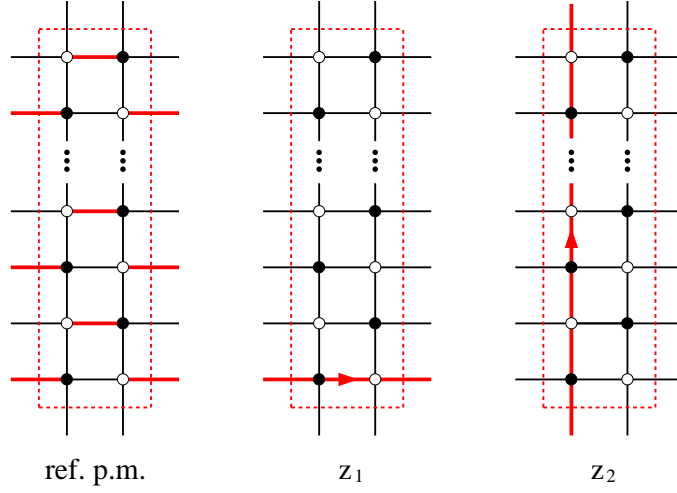


Figure 4: Reference perfect matching and z_1 and z_2 paths for $Y^{p,0}$.

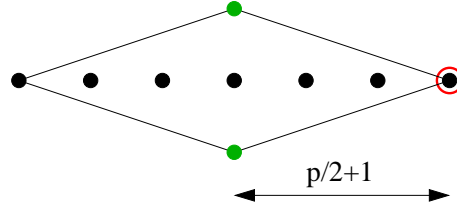


Figure 5: Toric diagram for $Y^{p,0}$ (shown in the figure for $p = 6$). The reference perfect matching is circled in red. By construction, its position in the (z_1, z_2) plane is $(0, 0)$. The green dots correspond to cycles with windings $(-p/2 - 1, 1)$ and $(-p/2 - 1, -1)$.

$$H_2 = (c_1 c_3 + c_2 c_4) + (c_1(d_3 + d_4) + c_2(d_4 + d_1) + c_3(d_1 + d_2) + c_4(d_2 + d_3)) \quad (4.4)$$

$$+ (d_1 d_2 + d_1 d_3 + d_1 d_4 + d_2 d_3 + d_3 d_4) ,$$

$$H_3 = (d_2 d_3 d_4 + d_1 d_3 d_4 + d_1 d_2 d_4 + d_1 d_2 d_3) + (c_1 d_3 d_4 + c_2 d_4 d_1 + c_3 d_1 d_2 + c_4 d_2 d_3) .$$

4.2 Kasteleyn matrix

Let us construct the Kasteleyn matrix for the dimer model in Figure 3. It is convenient to label edges according to whether they are horizontal (H and \tilde{H}) or vertical (V and

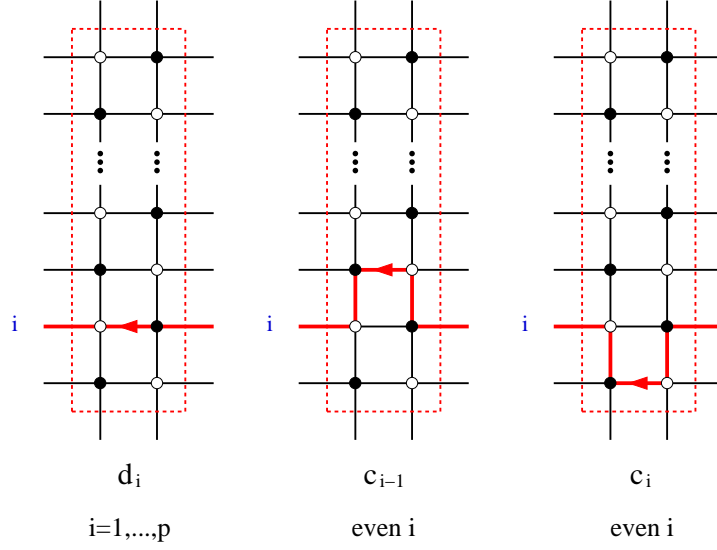


Figure 6: $2p$ of the cycles in a convenient basis for $Y^{p,0}$. Notice that the c cycles only exist for even i .

\tilde{V}). H edges are those at the center of the tiling and \tilde{H} are those crossing the edge of the unit cell. In addition:

V : vertical with black node at top endpoint
 \tilde{V} : vertical with white node at top endpoint

Finally, let us call H_i and \tilde{H}_i the edges connecting nodes i and $n+i$, $V_i \equiv V_{i+1,p+i}$ and $\tilde{V}_i \equiv \tilde{V}_{i,p+i+1}$. Subindices indicate nodes on the tiling and are identified mod($2p$). In these variables, the Kasteleyn matrix is

$$K_p = \begin{pmatrix} & p+1 & p+2 & p+3 & \cdots & 2p-1 & 2p \\ 1 & -H_1 - \tilde{H}_1 z_1 & \tilde{V}_1 & & & & V_p z_2 \\ 2 & V_1 & H_2 + \tilde{H}_2 z_1^{-1} & \tilde{V}_2 & & & \\ 3 & & V_2 & \ddots & & & \\ \vdots & & & & \ddots & & \\ p-1 & & & & & \ddots & \tilde{V}_{p-1} \\ p & \tilde{V}_p z_2^{-1} & & & & V_{p-1} & H_p + \tilde{H}_p z_1^{-1} \end{pmatrix} \quad (4.5)$$

Notice the alternating overall sign of the terms on the diagonal.

4.2.1 Non-Relativistic Limit

The Kasteleyn matrix (4.5) and the Lax operator of the non-relativistic periodic Toda chain [28, 29] are strikingly similar. We now make this connection explicit by first expressing the edge variables in terms of coordinates and momenta and then taking the non-relativistic (i.e. small momentum) limit.⁶ We define

$$\begin{aligned} V_i &= \tilde{V}_i \equiv e^{q_i - q_{i+1}} \\ H_i &= -\tilde{H}_i^{-1} \equiv e^{(-1)^i p_i / 2} \end{aligned} \quad (4.6)$$

and

$$z_1 \equiv e^{-z} \quad z_2 \equiv w \quad (4.7)$$

In the next section, we explain how these definitions and canonical Poisson brackets $\{p_i, q_j\} = \delta_{ij}$ are in agreement with the Goncharov-Kenyon Poisson brackets.⁷

Taking the small momenta limit (i.e. linear order in p_i and z) of the Kasteleyn matrix (4.5), we conclude that

$$\det K_p = \det(L_p(w) - z) \quad (4.8)$$

with

$$L_p(w) = \begin{pmatrix} p_1 & e^{q_1 - q_2} & & & e^{q_p - q_1} w \\ e^{q_1 - q_2} & p_2 & e^{q_2 - q_3} & & \\ & e^{q_2 - q_3} & \ddots & & \\ & & & \ddots & \\ & & & & \ddots & e^{q_{p-1} - q_p} \\ e^{q_p - q_1} w^{-1} & & & & e^{q_{p-1} - q_p} & p_p \end{pmatrix} \quad (4.9)$$

which is precisely the Lax operator of the non-relativistic periodic Toda chain. Notice that the previous analysis nicely associates coordinates and momenta with the vertical and horizontal directions of the square lattice, respectively.

4.2.2 Loop Poisson Brackets from Edges

In the previous section we have expressed edges of the brane tiling in term of coordinates and momenta in such a way that the Lax operator of the periodic Toda chain is obtained from the Kasteleyn matrix of the dimer model by taking the non-relativistic limit. We now show how the commutation relations among loop variables given by the Goncharov-Kenyon rules are recovered from our edge definitions and the $\{p_i, q_j\}$ Poisson brackets.

⁶The definitions in (4.6) are reasonable, rather symmetric and simple. We later check that they are indeed consistent with the w_i commutation relations.

⁷Changing from the basis of coordinates and momenta in (4.6) to the one in (4.3) is straightforward.

Consider $Y^{p,0}$ with even p . Using equation (2.3), we have

$$\begin{aligned} \text{odd } i: \quad w_i &= H_i \quad V_i^{-1} \quad H_{i+1} \quad \tilde{V}_i^{-1} & w_{p+i} &= \tilde{H}_i^{-1} \quad \tilde{V}_i \quad \tilde{H}_{i+1}^{-1} \quad V_i \\ \text{even } i: \quad w_i &= H_i^{-1} \quad V_i \quad H_{i+1}^{-1} \quad \tilde{V}_i & w_{p+i} &= \tilde{H}_i \quad \tilde{V}_i^{-1} \quad \tilde{H}_{i+1} \quad V_i^{-1} \end{aligned} \quad (4.10)$$

$i = 1, \dots, p$. From (4.10) and the canonical Poisson brackets $\{p_i, q_j\} = \delta_{ij}$ (which become $[p_i, q_j] = -i\hbar \delta_{ij}$ in the quantum theory) we can calculate

$$\frac{\{A, B\}}{AB} = \left(\begin{array}{c|cccccc|cccccc} & w_1 & w_2 & \cdots & \cdots & \cdots & w_p & w_{p+1} & w_{p+2} & \cdots & \cdots & \cdots & w_{2p} \\ \hline w_1 & & 2 & & & & 2 & -4 & & & & & \\ w_2 & -2 & & -2 & & & & & 4 & & & & \\ w_3 & & 2 & & & 2 & & & & -4 & & & \\ \vdots & & & \ddots & & \ddots & & & & & \ddots & & \\ w_{p-1} & & & & & 2 & 2 & & & & & -4 & \\ w_p & -2 & & & & & -2 & & & & & & 4 \\ \hline w_{p+1} & 4 & & & & & & -2 & & & & & -2 \\ w_{p+2} & & -4 & & & & & 2 & & 2 & & & \\ w_{p+3} & & & 4 & & & & & -2 & & -2 & & \\ \vdots & & & & \ddots & & & & & \ddots & & \ddots & \\ w_{2p-1} & & & & & & 4 & & & & -2 & & -2 \\ w_{2p} & & & & & & & -4 & 2 & & & & 2 \end{array} \right) \quad (4.11)$$

which, modulo an unimportant overall scaling, are exactly the Poisson brackets that follow from Goncharov-Kenyon prescription! This scaling can be absorbed in the value of \hbar in the quantum theory. It is important to notice that the final result depends crucially on the details of (4.6), such as the sign of the exponents, which are also vital for obtaining the correct non-relativistic limit. An interesting example that depends on these details is $\{w_i, w_{p+i+1}\} = 0$.⁸

4.3 More Relativistic Generalizations of Toda from $Y^{p,q}$

The integrable models based on $Y^{p,0}$ are not the only possible relativistic generalizations of the periodic Toda chain. In fact, as we now discuss, all $Y^{p,q}$ geometries give rise to valid generalizations. The corresponding toric diagram is shown Figure 7.⁹ These integrable systems were conjectured to exist in [30].

⁸Of course, the variables in (4.6) also reproduce the Poisson brackets (4.1) for the basis of cycles we considered in Section 4.1. Those cycles are typically written in terms of coordinates and momenta such that horizontal lines are equal to $e^{p'_i}$ and squares are equal to $e^{q'_i - q'_{i+1}}$. The p_i and q_i considered in this section are the ones in which the Lax operator takes the form (4.9), but can be mapped to p'_i and q'_i by an appropriate change of variables.

⁹The toric diagram in Figure 5 can be put into this form by an $SL(2, \mathbb{Z})$ transformation.

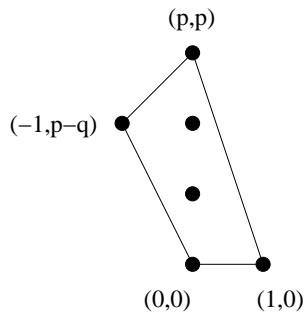


Figure 7: Toric diagram for the cone over $Y^{p,q}$.

M-theory on the CY cones over $Y^{p,q}$ geometries gives rise to 5d, $\mathcal{N} = 1$, pure $SU(p)$ gauge theories. The theories differ in the value of c_{cl} , which is a quantized parameter of the theory that controls the cubic couplings in the exact quantum prepotential, related to a five dimensional Chern-Simons term [19]. For $Y^{p,q}$, we have $c_{cl} = q$.

The distinction between theories with different values of c_{cl} disappears when taking the non-relativistic limit. This fact is clearly manifest at the level of the spectral curve. The spectral curve associated with $Y^{p,q}$ and the manipulations for taking its non-relativistic limit have repeatedly appeared in the literature (see for example [32], which we now follow).¹⁰ The spectral curve, Σ , can be written as

$$z_1 + \alpha \frac{z_2^{p-q}}{z_1} + P_p(z_2) = 0 \quad (4.12)$$

with $P_p(z_2)$ a degree p polynomial. We can rewrite Σ as

$$y^2 = \prod_{i=1}^p (z_2 - e^{\phi_i})^2 - 4e^{-t_B} z_2^{p-q} \quad (4.13)$$

In order to take the non-relativistic (4d) limit, we define

$$z_2 = e^{\beta x}, \quad e^{\phi_i} = e^{\beta a_{i,i+1}}, \quad e^{-t_B} = \left(\frac{\beta \Lambda}{2}\right)^{2p}, \quad (4.14)$$

with $a_{i,i+1} = a_i - a_{i+1}$. From our perspective, it is clear that not only z_2 but also the ϕ_i variables and t_B must be rescaled when taking the non-relativistic limit since they are controlled by the w_i variables, which are momentum dependent. In the $\beta \rightarrow 0$ limit, Σ

¹⁰In fact, this correspondence of the spectral curve is the original reason why we identify $Y^{p,q}$ dimer models as giving rise to relativistic generalizations of the periodic Toda chain.

becomes

$$y^2 = \prod_{i=1}^p (x - a_{i,i+1})^2 - 4 \left(\frac{\Lambda}{2} \right)^{2p}, \quad (4.15)$$

which is the Seiberg-Witten curve for the pure $\mathcal{N} = 2$ $SU(N)$ gauge theory. As we have anticipated, the dependence on q has disappeared. Reversing the reasoning, we conclude that all $Y^{p,q}$ manifolds (i.e. for arbitrary values of q) give rise to integrable systems that can be considered relativistic generalizations of the periodic Toda chain. In the next section we discuss the $Y^{p,p}$ geometry and its corresponding integrable system.

4.4 $Y^{p,p}$ Integrable Systems

We now construct a new infinite family of relativistic integrable systems associated with $Y^{p,p}$. From the discussion in section 4.3, we know that these systems also reduce to the periodic Toda chain in the non-relativistic limit.

The cone over $Y^{p,p}$ is the $\mathbb{C}^3/\mathbb{Z}_{2p}$ orbifold. Its brane tiling consist of two columns of p hexagons [6] as shown in Figure 8.

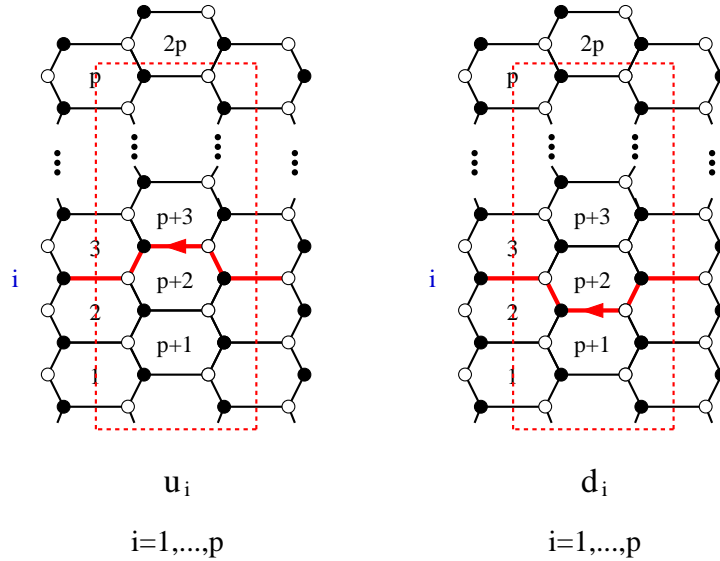


Figure 8: Brane tiling for $Y^{p,p}$. A convenient basis for $Y^{p,p}$ is given by the u_i (up) and d_i (down) cycles, $i = 1, \dots, p$.

Figure 9 shows the toric diagram for $Y^{p,p}$, where the reference perfect matching is indicated with a red circle. As for $Y^{p,0}$, the analysis of these models is simplified by a convenient choice of basis for closed cycles. Figure 8 shows $2p$ of them. There are

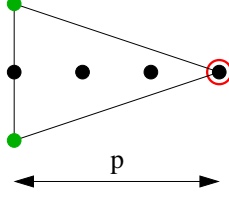


Figure 9: Toric diagram for $Y^{p,p}$ (shown in the figure, $p = 3$). The reference perfect matching is circled in red. By construction, its position in the (z_1, z_2) plane is $(0, 0)$. The green dots correspond to cycles with windings $(-p, 1)$ and $(-p, -1)$.

two additional cycles with windings $(-p, 1)$ and $(-p, -1)$ along the (z_1, z_2) directions. They correspond to the green points in Figure 9 and are fixed by the Casimirs.

The Hamiltonian associated to the $(-1, 0)$ point in the toric diagram takes the simple form

$$H_1 = \sum_{i=1}^p (u_i + d_i). \quad (4.16)$$

Similar to our analysis of $Y^{p,0}$, determining the Hamiltonians for the $(-n, 0)$ points is very simple in the u_i and d_i basis. Finding the n^{th} Hamiltonian reduces to determining all possible combinations of n cycles that do not overlap or intersect at nodes of the tiling. For example, the higher Hamiltonians for $Y^{4,4}$ are

$$\begin{aligned} H_2 = & u_1u_2 + u_1u_3 + u_1u_4 + u_2u_3 + u_2u_4 + u_3u_4 \\ & + d_1d_2 + d_1d_3 + d_1d_4 + d_2d_3 + d_2d_4 + d_3d_4 \\ & + u_1d_3 + u_1d_4 + u_2d_4 + u_2d_1 + u_3d_1 + u_3d_2 + u_4d_2 + u_4d_3, \end{aligned}$$

$$\begin{aligned} H_3 = & u_1u_2u_3 + u_1u_2u_4 + u_1u_3u_4 + u_2u_3u_4 \\ & + u_1d_3d_4 + u_2d_4d_1 + u_3d_1d_2 + u_4d_2d_3 \\ & + d_1d_2d_3 + d_1d_2d_4 + d_1d_3d_4 + d_2d_3d_4 \\ & + d_1u_2u_3 + d_2u_3u_4 + d_3u_4u_1 + d_4u_1u_2, \end{aligned}$$

$$H_4 = u_1u_2u_3u_4 + d_1d_2d_3d_4. \quad (4.17)$$

4.5 $Y^{p,q}$ Integrable Systems as Spin Chains

We have identified the family of integrable systems associated to the $Y^{p,q}$ dimer models in the previous section. Previously the integrable systems identified with the $Y^{p,q}$

spectral curves were described as twisted $\mathfrak{sl}(2)$ XXZ spin chains with impurities [33]. We will now explain the equivalence of these apparently different descriptions.

The $\mathfrak{sl}(2)$ spin chains are described by N “spins” Ψ_i where $i = 1, \dots, N$. The spin operators satisfy the commutation relations

$$\{S_{\pm}, S_0\} = \pm S_{\pm}, \quad \{S_+, S_-\} = \sinh 2S_0$$

where the raising and lowering operators $S_{\pm} = S_1 \pm iS_2$ are defined as usual. Integrability of the spin chain can be shown starting from the auxiliary linear problem for the Lax matrix

$$L_i(\mu)\Psi_i(\mu) = \Psi_{i+1}(\mu)$$

with twisted boundary conditions implemented by the identification

$$\Psi_{i+N}(\mu) = -w\Psi_i(\mu).$$

The spectral curve of the spin chain is given by the determinant of the transfer matrix,

$$\det(T(\lambda) + w1) = 0,$$

where the transfer matrix is defined by the product of the two-by-two Lax matrices

$$T(\lambda) \equiv L_N(\lambda) \dots L_1(\lambda).$$

Impurities are added to the spin chain by performing a site-dependent shift of variables for the Lax matrices $L_j(\mu)$. $Y^{p,q}$ quiver gauge theories can be constructed by starting from $Y^{p,p}$ and adding $(p - q)$ impurities [22]. Amusingly, the spin chain and quiver impurities are precisely the same. This reflects the well-known phenomena that the same integrable system can have different Lax representations. Since the Lax matrices for all of the $Y^{p,q}$ quiver gauge theories are tridiagonal [6], we can re-write the determinant of the Lax matrix in spin-chain form using the following identity

$$\det \begin{pmatrix} a_1 & b_1 & & c_0 \\ c_1 & \ddots & \ddots & \\ & \ddots & \ddots & b_{N-1} \\ b_0 & & c_{N-1} & a_N \end{pmatrix} = (-1)^{N-1} \left(\prod_j b_j + \prod_j c_j \right) + \text{Tr} L_N L_{N-1} \dots L_1$$

where

$$L_j = \begin{pmatrix} a_j & -b_{j-1}c_{j-1} \\ 1 & 0 \end{pmatrix}.$$

Thus we can re-write the the spectral curve as

$$\det(T(\lambda) + w1) = w^2 + w\text{Tr}T(\lambda) + \det T(\lambda).$$

Under a suitable change of variables, it should be straightforward to show that this representation matches the XXZ form proposed in [33]. For the relativistic, periodic Toda chain this change of variables appears in [31].

5. Generating New Integrable Systems via Partial Resolution

In this section we explain how to determine the integrable system associated with a partial resolution, given the one for the parent theory. This is a useful way of obtaining new integrable systems from known ones. Starting from a relatively complicated example, partial resolution provides a practical way of deriving new integrable systems, much faster in practice than going through the process of expressing the new system in terms of loop variables. This method is so efficient that it is natural to expect that it has a counterpart in the integrable system literature.

We will focus on minimal partial resolutions, which correspond to removing extremal perfect matchings (i.e those located at corners of the toric diagram) one at a time.¹¹ In addition, it might be necessary to simultaneously remove non-extremal perfect matchings. The result of this process is a new toric diagram in which the multiplicity of each new extremal perfect matching is one and some of the internal multiplicities might also change. From a quiver point of view, partial resolution corresponds to turning on non-zero vacuum expectation values (vevs) for bifundamental fields X_{ij} and then higgsing nodes i and j .¹² This operation might result in mass terms for some fields, which can be integrated out using their equations of motion. From a dimer model perspective, partial resolution corresponds to removing from the tiling the edges associated to the fields with non-zero vevs. As a result, some of the adjacent faces in the tiling are merged into a single new face. The integration of massive fields maps to the removal of 2-valent vertices that might be generated in the process by condensing the nodes at the endpoints of the two edges terminating in them.

The standard understanding of partial resolutions using dimer models is that all perfect matchings containing the edge associated with X_{ij} are removed [6]. Following the connection between bifundamental fields and perfect matchings given in [6], we see that all these perfect matchings (which are interpreted as GLSM fields) need to acquire a non-zero vev in order for the bifundamental to get one.

¹¹The implementation of more general partial resolutions using dimer models has been discussed in great detail in [34]. We will restrict ourselves to minimal ones in this paper.

¹²Notice that, given a quiver, not all possible higgsings correspond to consistent partial resolutions.

In the integrable systems context, the fundamental objects are closed loops rather than individual perfect matchings. In fact, even the reference perfect matching might disappear when applying the discussion in the previous paragraph. It is straightforward to adapt the previous reasoning to loops: partial resolution removes all loops that contain an edge that gets a non-zero vev.

From a brane tiling perspective, the edge associated to X_{ij} is deleted and faces i and j are combined into a single face. Consequently, we start from two cycles w_i and w_j and end with a combined cycle $w_{i/j} = w_i w_j$ as shown in Figure 10.

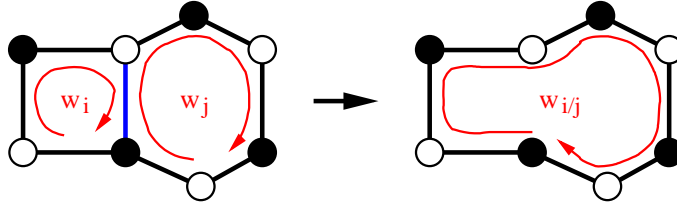


Figure 10: Combination of gauge group cycles when higgsing by a vev associated to the blue edge.

The following rules produce the integrable system for the partially resolved geometry:

- 1) Remove loops that contain an edge with a non-zero vev.
- 2) Re-express the surviving loops with the replacement $(w_i w_j) \rightarrow w_{i/j}$.

More practically, the loops that are removed in rule (1) are those that cannot be re-written using rule (2).

In some cases, a z_i path can involve an edge that is removed when higgsing, as shown in Figure 11. If so, the path can be redefined by using a w_j to make the path wiggle appropriately, avoiding this edge. Equivalently, we could have chosen a different set of z_i paths in the parent theory such that they do not involve higgsed edges.

5.1 Examples: Partial Resolutions of $Y^{4,0}$

We now illustrate our ideas in the explicit case of partial resolutions of $Y^{4,0}$. Partial resolution can either preserve or reduce the genus of the spectral curve (i.e. the number of Hamiltonians). The examples that follow exhibit the latter behavior.

In this section we depart from the notation for edges we used for general $Y^{p,0}$ in Section 4.2, which was specially devised for giving the Kasteleyn matrix a nice form.

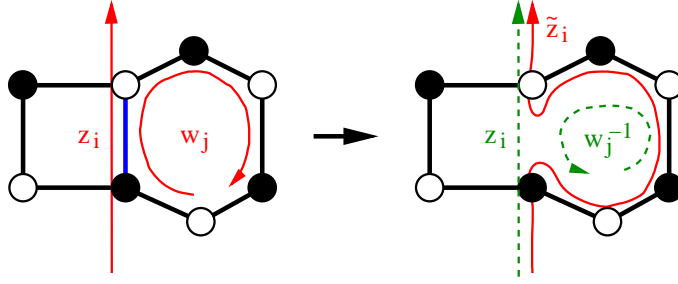


Figure 11: Redefinition of one of the paths that winds around the \mathbb{T}^2 , $z_i = \tilde{z}_i w_j$, after partial resolution by turning on a vev for the blue edge.

Here our emphasis is on higgsing, so we explicitly indicate the gauge groups under which bifundamentals are charged using subindices. V_{ij} and \tilde{V}_{ij} indicate vertical edges in the first and second columns of the brane tiling, respectively. Horizontal edges are denoted H_{ij} .

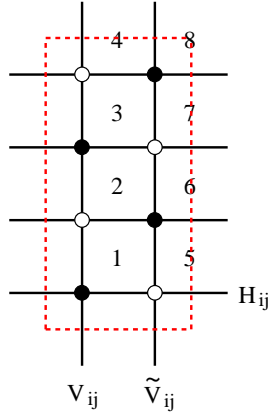


Figure 12: Brane tiling for $Y^{4,0}$.

Figure 13 shows the resolutions we will consider. The number of gauge groups in the associated quivers is given by twice the area of the toric diagrams. This implies that the number of bifundamental expectation values that need to be turned on is equal to twice the decrease in area of the toric diagram.

The starting point is the integrable system for $Y^{4,0}$. In the table below, (n_1, n_2) gives the $(z_1^{n_1} z_2^{n_2})$ contribution. Every term in a given contribution arises from a loop in the tiling or equivalently from a perfect matching. Hamiltonians correspond to internal points and Casimirs are given by the ratio of consecutive points on the boundary.

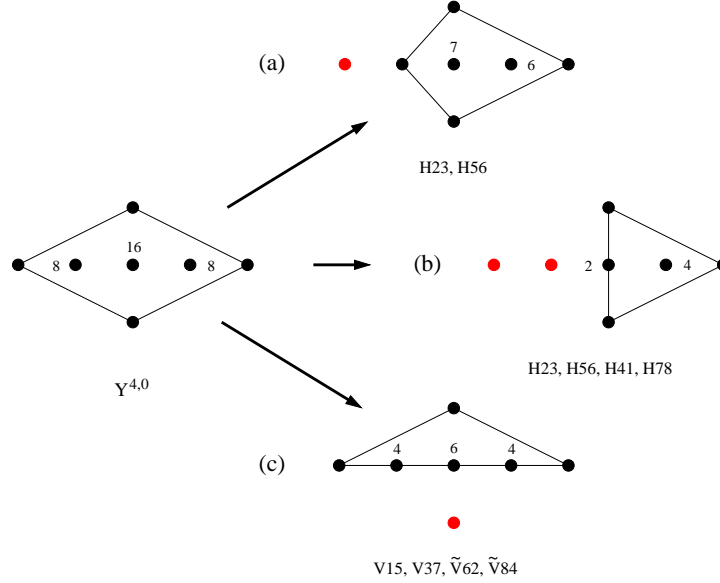


Figure 13: Toric diagrams for $Y^{4,0}$ and various of its partial resolutions. We indicate the multiplicity associated with each point and the non-zero vevs that need to be turned on. Higgsing takes the number of Hamiltonians from 3 in the original theory to a) 2, b) 1 and c) 0.

Instead of the basis of cycles used in Section 4.1, here we use the w_i (which correspond to gauge groups), z_1 and z_2 basis, since it makes higgsing more transparent.

(n_1, n_2)	Loops
$(0, 0)$	1
$(-1, 0)$	$w_4 + w_4w_8 + w_4w_7w_8 + w_3w_4w_7w_8 + w_2w_3w_4w_7w_8$ $+w_2w_3w_4w_6w_7w_8 + w_2w_3w_4w_5w_6w_7w_8 + 1$
$(-2, 0)$	$w_1^{-1}w_5^{-1}w_4 + w_4w_8 + w_1^{-1}w_4w_8 + w_1^{-1}w_5^{-1}w_4w_8$ $+w_1^{-1}w_5^{-1}w_6^{-1}w_4w_8 + w_4w_7w_8 + w_1^{-1}w_4w_7w_8 + w_1^{-1}w_5^{-1}w_4w_7w_8$ $+w_3w_4w_7w_8 + w_1^{-1}w_3w_4w_7w_8 + w_1^{-1}w_5^{-1}w_3w_4w_7w_8 + w_2w_3w_4w_7w_8$ $+w_1^{-1}w_5^{-1} + w_3w_4^2w_7w_8 + w_2w_3w_4^2w_7w_8 + w_3w_4^2w_7w_8^2$
$(-3, 0)$	$w_1^{-1}w_5^{-1}w_4w_8 + w_1^{-1}w_5^{-1}w_6^{-1}w_4w_8 + w_1^{-1}w_5^{-1}w_4w_7w_8 + w_1^{-1}w_5^{-1}w_3w_4w_7w_8$ $+w_1^{-1}w_5^{-1}w_3w_4^2w_7w_8 + w_3w_4^2w_7w_8^2 + w_1^{-1}w_3w_4^2w_7w_8^2 + w_1^{-1}w_5^{-1}w_3w_4^2w_7w_8^2$
$(-4, 0)$	$w_1^{-1}w_5^{-1}w_3w_4^2w_7w_8^2$
$(-2, 1)$	$w_1^{-1}w_4w_7w_8$
$(-2, -1)$	$w_2w_3w_4^2w_7w_8$

(5.1)

Higgsing a

Model (a) in Figure 13 is obtained by giving non-zero vevs to both H_{23} and H_{56} . There are other choices of expectation values that lead to the same result. Figure 14 shows the corresponding brane tiling.

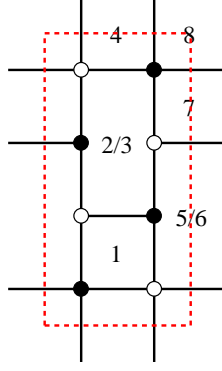


Figure 14: Brane tiling for model (a) obtained by higgsing $Y^{4,0}$.

The resulting integrable model is given by:

(n_1, n_2)	Loops
$(0, 0)$	1
$(-1, 0)$	$w_4 + w_4w_8 + w_4w_7w_8 + w_{2/3}w_4w_7w_8$ $+w_{2/3}w_4w_{5/6}w_7w_8 + 1$
$(-2, 0)$	$w_4w_8 + w_1^{-1}w_4w_8 + w_1^{-1}w_{5/6}^{-1}w_4w_8 + w_4w_7w_8$ $+w_1^{-1}w_4w_7w_8 + w_{2/3}w_4w_7w_8 + w_{2/3}w_4^2w_7w_8$
$(-3, 0)$	$w_1^{-1}w_{5/6}^{-1}w_4w_8$
$(-2, 1)$	$w_1^{-1}w_4w_7w_8$
$(-2, -1)$	$w_{2/3}w_4^2w_7w_8$

(5.2)

Higgsing b

Model (b) corresponds to turning on vevs for H_{23} , H_{56} , H_{78} and H_{41} . The resulting brane tiling is shown in Figure 15.

The edge associated to H_{41} is contained in the original z_1 path, which thus needs to be redefined. We can consider a new path \tilde{z}_1 given by $z_1 = \tilde{z}_1w_1^{-1}$. The integrable system is summarized in (5.3), where now (n_1, n_2) corresponds to the $(\tilde{z}_1^{n_1} z_2^{n_2})$ contributions.

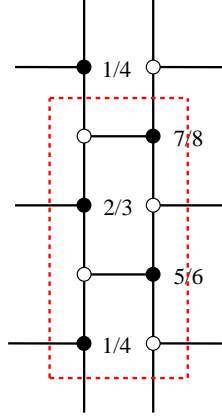


Figure 15: Brane tiling for model (b) obtained by higgsing $Y^{4,0}$.

(n_1, n_2)	Loops
$(0, 0)$	1
$(-1, 0)$	$w_{4/1} + w_{4/1}w_{7/8} + w_{2/3}w_{4/1}w_{7/8} + w_{2/3}w_{4/1}w_{5/6}w_{7/8}$
$(-2, 0)$	$w_{4/1}w_{7/8} + w_{2/3}w_{4/1}^2w_{7/8}$
$(-2, 1)$	$w_{4/1}w_{7/8}$
$(-2, -1)$	$w_{2/3}w_{4/1}^2w_{7/8}$

(5.3)

Higgsing c

Finally, model (c) follows from turning on vevs for V_{15} , V_{37} , \tilde{V}_{62} and \tilde{V}_{84} . The corresponding brane tiling is shown in Figure 16.

This time both V_{15} and V_{37} overlap with the original z_2 path, which can be redefined according to $z_2 = \tilde{z}_2 w_1 w_3$. Denoting (n_1, n_2) the $(z_1^{n_1} \tilde{z}_2^{n_2})$ contribution, (5.4) summarizes the resulting integrable system.

(n_1, n_2)	Loops
$(0, 0)$	1
$(-1, 0)$	$w_{8/4} + w_{3/7}w_{8/4} + w_{6/2}w_{3/7}w_{8/4} + 1$
$(-2, 0)$	$w_{8/4} + w_{1/5}^{-1}w_{8/4} + w_{3/7}w_{8/4} + w_{1/5}^{-1}w_{3/7}w_{8/4} + w_{1/5}^{-1} + w_{3/7}w_{8/4}^2$
$(-3, 0)$	$w_{1/5}^{-1}w_{8/4} + w_{1/5}^{-1}w_{3/7}w_{8/4} + w_{3/7}w_{8/4}^2 + w_{1/5}^{-1}w_{3/7}w_{8/4}^2$
$(-4, 0)$	$w_{1/5}^{-1}w_{3/7}w_{8/4}^2$
$(-2, 1)$	$w_{3/7}w_{8/4}$

(5.4)

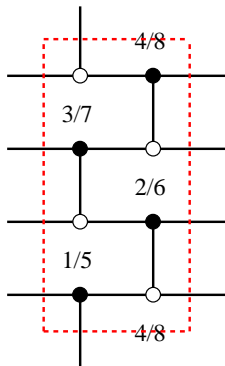


Figure 16: Brane tiling for model (c) obtained by higgsing $Y^{4,0}$.

From an integrability point of view, this model is trivial, i.e. it only consists of Casimirs. From a quiver perspective, the reason for this is that, as one can deduce from Figure 16, the associated quiver is fully non-chiral. This implies that all commutators vanish.

6. Conclusions and Outlook

We have investigated various applications of the correspondence between dimer models and integrable system introduced by Goncharov and Kenyon in [5]. We used it to explicitly construct relativistic generalizations of the periodic Toda chain associated to $Y^{p,0}$ and $Y^{p,p}$ geometries. In these models, the calculation of commuting Hamiltonians reduces to the combinatorics of non-intersecting paths on the brane tiling. We investigated the connection between the Kasteleyn matrix and the Lax operator, the non-relativistic limit of the integrable systems, additional relativistic versions of the periodic Toda chain based dimer models for general $Y^{p,q}$ geometries, and the identification of quiver impurities and spin chain impurities. Finally, we introduced a method for generating new integrable systems based on higgsing. We can envision, and are currently pursuing, multiple directions in which the correspondence between dimer models and integrable systems can be exploited. We discuss some of them below.

We have explained how higgsing is an efficient tool for generating new integrable systems. The characteristic polynomials for the dimer models associated to $\mathbb{Z}_n \times \mathbb{Z}_m$ orbifolds of arbitrary geometries, which correspond to $n \times m$ arrays of copies of the original unit cell, can be determined using simple formulas [10]. These expressions have been used for calculating the multiplicity of perfect matchings associated to points in the toric diagrams of orbifolds [23]. It would be interesting to investigate whether there are

analogous expressions for the integrable systems associated to orbifolds starting from the integrable system for the unorbifolded geometry. New integrable systems could then be generated by higgsing, using the orbifold theories as starting points.

It would be interesting to study the continuous limit of integrable systems arising from dimer models. By this, we not only mean the infinite length limit of integrable chains but also the (1+1)-dimensional field theory limit of fixed length systems. It is reasonable to conjecture that field theories such as A_n Toda field theories can be constructed in this way. Furthermore, it is natural to expect that dimer models are useful for classifying (0+1)-dimensional, integrability-preserving defects and interfaces that can be added to such field theories.

The work of [35] investigated the quantization of Riemann surfaces defined by the vanishing of the A-polynomials of three-manifolds M that are the complement of (thickened) knots or links. In the case of knots, the boundary of M is a 2-torus. The decomposition of M into glued tetrahedra with truncated vertices gives rise to a triangulation of the 2-torus, the developing map, whose dual is reminiscent of a dimer model. On the other hand, [5] and [8] discussed the relation between dimer models and quantum Teichmüller space. It is then natural to ask whether the existing similarities indicate the existence of a true connection that associates dimer models to three-manifolds that are knot complements.

One clear direction for further research is to explore the connection between quantum integrable systems and gauge theories proposed by Nekrasov and Shatashvili [2]. By considering the 5d gauge theory on an Ω -background with $\epsilon_1 = \epsilon$ and $\epsilon_2 = 0$, the classical integrable systems we have investigated become quantized. We now review the interpretation of the quantization in terms of a B-brane on the spectral curve using the refined topological string [36]. The mirror Calabi-Yau geometry takes the form

$$uv + H(x, p) = 0.$$

When the Ω -background is turned on, the classical spectral curve, Σ defined by $H(x, p) = 0$, is promoted to a quantum spectral curve

$$\hat{H}(x, p)\Psi(x) = 0$$

where $\Psi(x)$ is the wave-function for a B-brane. The quantum spectral curve is the Baxter equation for the relativistic Toda chain [31]. The coefficients of $H(x, p)$ are the energy eigenvalues of the Hamiltonians (and Casimirs) of the quantum integrable system. In the relativistic case, the differential operators $e^{\hat{p}}$ become shift operators, acting on $\Psi(x)$ by

$$e^{\hat{p}}\Psi(x) \rightarrow \Psi(x + \hbar).$$

Solutions to this differential equation were obtained from the refined topological string partition function in [36]. Thus the refined topological string should provide a way to solve the Baxter equation for quantum integrable systems. We plan to elucidate this connection in future work.

A graphical representation for the finite non-periodic Toda lattice, similar to dimer models, was developed [37] using the Poisson geometry of planar directed networks in an annulus [38]. The geometry of planar directed networks was developed in order to study the totally nonnegative Grassmannian [44]. Our work suggests an intriguing connection between the geometry of brane tilings and the totally nonnegative part of the double loop Grassmannian.

In general, gauge theories arising from brane tilings have sequences of periodic Seiberg dualities known as duality cascades [39]-[43]. According to [5], Seiberg dualities correspond to canonical transformations of the integrable system. In terms of the new variables the Hamiltonians will typically take a different functional form. However, since cascades are periodic, we are interested in special canonical transformations that preserve the functional form of the commuting Hamiltonians. Such canonical transformations are known as auto-Bäcklund-Darboux transformations. For example, the transformation [45]

$$\tilde{c}_i = c_i \frac{d_i + c_{i-1}}{d_{i+1} + c_i}, \quad \tilde{d}_i = d_{i+1} \frac{d_i + c_{i-1}}{d_{i+1} + c_i}$$

is an auto-Bäcklund-Darboux transformation of the relativistic Toda chain because it is canonical and the new Hamiltonian

$$\tilde{H} = \sum_i (\tilde{c}_i + \tilde{d}_i)$$

takes the same functional form as the original Hamiltonian. The theory of auto-Bäcklund-Darboux transformations is closely related to the theory of separation of variables and discrete-time integrable systems [46, 47]. Thus we expect a fruitful interplay between duality cascades and integrable systems.

Acknowledgments

We would like to thank Y. H. He and D. Morrison for useful discussions. We also thank D. Morrison for reading the manuscript. We are particularly grateful to M. Aganagic for early collaboration and insightful discussions. S. F. would like to thank to A. Goncharov and R. Kenyon for sharing a draft of [5] before its publication. The work of R. E. is supported in part by the National Science Foundation under grant DMS-1007414 and by the World Premier International Research Center Initiative (WPI

Initiative), MEXT, Japan. S. F. is supported by the National Science Foundation under Grant No. PHY05-51164. The work of K. S. is supported by the Berkeley Center for Theoretical Physics.

References

- [1] A. Gorsky, I. Krichever, A. Marshakov, A. Mironov, A. Morozov, “Integrability and Seiberg-Witten exact solution,” *Phys. Lett.* **B355**, 466-474 (1995). [hep-th/9505035].
- [2] N. A. Nekrasov, S. L. Shatashvili, “Quantization of Integrable Systems and Four Dimensional Gauge Theories,” [arXiv:0908.4052 [hep-th]].
- [3] N. Gromov, V. Kazakov, A. Kozak, P. Vieira, “Exact Spectrum of Anomalous Dimensions of Planar $N = 4$ Supersymmetric Yang-Mills Theory: TBA and excited states,” *Lett. Math. Phys.* **91**, 265-287 (2010). [arXiv:0902.4458 [hep-th]].
- [4] L. F. Alday, J. Maldacena, A. Sever, P. Vieira, “Y-system for Scattering Amplitudes,” *J. Phys. A* **A43**, 485401 (2010). [arXiv:1002.2459 [hep-th]].
- [5] A. Goncharov and R. Kenyon, “Dimers and cluster integrable systems,” to appear.
- [6] S. Franco, A. Hanany, K. D. Kennaway, D. Vegh and B. Wecht, “Brane Dimers and Quiver Gauge Theories,” *JHEP* **0601**, 096 (2006) [arXiv:hep-th/0504110].
- [7] B. Feng, Y. -H. He, K. D. Kennaway, C. Vafa, “Dimer models from mirror symmetry and quivering amoebae,” *Adv. Theor. Math. Phys.* **12**, 3 (2008). [hep-th/0511287].
- [8] S. Franco, “Dimer Models, Integrable Systems and Quantum Teichmuller Space,” [arXiv:1105.1777 [hep-th]].
- [9] B. Feng, S. Franco, A. Hanany and Y. H. He, “Symmetries of toric duality,” *JHEP* **0212**, 076 (2002) [arXiv:hep-th/0205144].
- [10] R. Kenyon, A. Okounkov and S. Sheffield, “Dimers and Amoebae,” arXiv:math-ph/0311005.
- [11] S. Franco and D. Vegh, “Moduli spaces of gauge theories from dimer models: Proof of the correspondence,” *JHEP* **0611**, 054 (2006) [arXiv:hep-th/0601063].
- [12] N. Nekrasov, “Five dimensional gauge theories and relativistic integrable systems,” *Nucl. Phys. B* **531**, 323 (1998) [arXiv:hep-th/9609219].
- [13] N. Seiberg, E. Witten, “Electric - magnetic duality, monopole condensation, and confinement in $N=2$ supersymmetric Yang-Mills theory,” *Nucl. Phys.* **B426**, 19-52 (1994). [hep-th/9407087].

- [14] N. Seiberg, E. Witten, “Monopoles, duality and chiral symmetry breaking in N=2 supersymmetric QCD,” Nucl. Phys. **B431**, 484-550 (1994). [hep-th/9408099].
- [15] O. Aharony, A. Hanany and B. Kol, “Webs of (p,q) 5-branes, five dimensional field theories and grid diagrams,” JHEP **9801**, 002 (1998) [arXiv:hep-th/9710116].
- [16] D. R. Morrison, N. Seiberg, “Extremal transitions and five-dimensional supersymmetric field theories,” Nucl. Phys. **B483**, 229-247 (1997). [hep-th/9609070].
- [17] M. R. Douglas, S. H. Katz, C. Vafa, “Small instantons, Del Pezzo surfaces and type I-prime theory,” Nucl. Phys. **B497**, 155-172 (1997). [hep-th/9609071].
- [18] O. J. Ganor, D. R. Morrison, N. Seiberg, “Branes, Calabi-Yau spaces, and toroidal compactification of the N=1 six-dimensional E(8) theory,” Nucl. Phys. **B487**, 93-127 (1997). [hep-th/9610251].
- [19] K. A. Intriligator, D. R. Morrison, N. Seiberg, “Five-dimensional supersymmetric gauge theories and degenerations of Calabi-Yau spaces,” Nucl. Phys. **B497**, 56-100 (1997). [hep-th/9702198].
- [20] I. Antoniadis, S. Ferrara, T. R. Taylor, “N=2 heterotic superstring and its dual theory in five-dimensions,” Nucl. Phys. **B460**, 489-505 (1996). [arXiv:hep-th/9511108 [hep-th]].
- [21] S. N. M. Ruijsenaars, “Finite-Dimensional Soliton Systems, in Integrable and Super-Integrable Systems, Ed. B.A. Kupershmidt, World Scientific, Singapore (1989).
- [22] S. Benvenuti, S. Franco, A. Hanany, D. Martelli, J. Sparks, “An Infinite family of superconformal quiver gauge theories with Sasaki-Einstein duals,” JHEP **0506**, 064 (2005). [hep-th/0411264].
- [23] A. Hanany, K. D. Kennaway, “Dimer models and toric diagrams,” [hep-th/0503149].
- [24] S. Kharchev, D. Lebedev, M. Semenov-Tian-Shansky, “Unitary representations of $U(q)$ ($\mathfrak{sl}(2, \mathbb{R})$), the modular double, and the multiparticle q deformed Toda chains,” Commun. Math. Phys. **225**, 573-609 (2002). [hep-th/0102180].
- [25] I. G. Korepanov, “Vacuum Curves, Classical Integrable Systems in Discrete Space-Time and Statistical Physics,” Zap. Nauchn. Semin. **235** (1996) 272 [arXiv:hep-th/9312197].
- [26] M. Bruschi and O. Ragnisco, “Lax representation and complete integrability for the periodic relativistic Toda lattice,”
- [27] S. Kharchev, D. Lebedev and M. Semenov-Tian-Shansky, “Unitary representations of $U_q(\mathfrak{sl}(2, \mathbb{R}))$, the modular double, and the multiparticle q-deformed Toda chains,” Commun. Math. Phys. **225**, 573 (2002) [arXiv:hep-th/0102180].

- [28] H. Flaschka, “The Toda lattice. I. Existence of integrals,” *Phys. Rev. B* (3), 9:1924–1925, 1974.
- [29] H. Flaschka, “On the Toda lattice. II. Inverse-scattering solution,” *Progr. Theoret. Phys.*, 51:703–716, 1974.
- [30] A. Brini and A. Tanzini, “Exact Results for Topological Strings on Resolved $Y^{p,q}$ Singularities,” *Commun. Math. Phys.* **289** (2009) 205 [arXiv:0804.2598 [hep-th]].
- [31] V. B. Kuznetsov, A. V. Tsyganov, “Separation of variables for the quantum relativistic Toda lattices,” [hep-th/9402111].
- [32] T. J. Hollowood, A. Iqbal and C. Vafa, “Matrix Models, Geometric Engineering and Elliptic Genera,” *JHEP* **0803**, 069 (2008) [arXiv:hep-th/0310272].
- [33] A. Gorsky, S. Gukov, and A. Mironov. SUSY field theories, integrable systems and their stringy/brane origin. II. *Nucl. Phys.*, B518:689–713, 1998.
- [34] I. Garcia-Etxebarria, F. Saad and A. M. Uranga, “Quiver gauge theories at resolved and deformed singularities using dimers,” *JHEP* **0606**, 055 (2006) [arXiv:hep-th/0603108].
- [35] T. Dimofte, “Quantum Riemann Surfaces in Chern-Simons Theory,” [arXiv:1102.4847 [hep-th]].
- [36] M. Aganagic, M. C. N. Cheng, R. Dijkgraaf, D. Krefl, C. Vafa, “Quantum Geometry of Refined Topological Strings,” [arXiv:1105.0630 [hep-th]].
- [37] M. Gekhtman, M. Shapiro, and A. Vainshtein, “Generalized Bäcklund–Darboux transformations for Coxeter–Toda flows from a cluster algebra perspective,” *Acta Mathematica*, 206:245–310, 2010. 10.1007. [arXiv:0906.1364 [math.QA]].
- [38] M. Gekhtman, M. Shapiro, and A. Vainshtein, “Poisson geometry of directed networks in an annulus,” [arXiv:0901.0020 [math.QA]].
- [39] I. R. Klebanov, M. J. Strassler, “Supergravity and a confining gauge theory: Duality cascades and chi SB resolution of naked singularities,” *JHEP* **0008**, 052 (2000). [arXiv:hep-th/0007191 [hep-th]].
- [40] S. Franco, A. Hanany, Y. -H. He, P. Kazakopoulos, “Duality walls, duality trees and fractional branes,” [hep-th/0306092].
- [41] S. Franco, Y. -H. He, C. Herzog, J. Walcher, “Chaotic duality in string theory,” *Phys. Rev.* **D70**, 046006 (2004). [hep-th/0402120].
- [42] C. P. Herzog, Q. J. Ejaz, I. R. Klebanov, “Cascading RG flows from new Sasaki-Einstein manifolds,” *JHEP* **0502**, 009 (2005). [hep-th/0412193].

- [43] S. Franco, A. Hanany, A. M. Uranga, “Multi-flux warped throats and cascading gauge theories,” *JHEP* **0509**, 028 (2005). [hep-th/0502113].
- [44] A. Postnikov, “Total positivity, grassmannians, and networks,” [math/0609764].
- [45] L. Faybusovich and M. Gekhtman, “Elementary Toda orbits and integrable lattices,” *J. Math. Phys.*, 41(5):2905–2921, 2000.
- [46] A. P. Veselov, “Integrable mappings,” *Uspekhi Mat. Nauk*, 46(5(281)):3–45, 190, 1991.
- [47] V. B. Kuznetsov and E. K. Sklyanin, “On bäcklund transformations for many-body systems,” *Journal of Physics A: Mathematical and General* **31** (1998), no. 9, 2241.